**Anomalous mixed crystals: a peculiar case of adsorption/absorption**

# Anomalous mixed crystals: a peculiar case of adsorption/absorption

**Dino Aquilano and Linda Pastero**

Università degli Studi di Torino
Dipartimento di Scienze Mineralogiche e Petrologiche
Via Valperga Caluso, 35 – 10125 Torino (Italy)

According to the Kern's lectures (this book), a peculiar form of incorporation named " anomalous mixed crystals" is known since the works by Johnsen [1], Gaubert [2], Neuhaus [3] and Seifert [4]. This kind of crystals is different from the "traditional mixed crystals" which are either zoned or sector-grown. As a matter of fact, the impurity entering the anomalous mixed crystals is distributed as thin lamellae parallel oriented to one or more faces of the matrix-crystal. Hence the system is bi-phased. Usually these lamellae are so thin that they can be revealed only by the anomalous optical bi-refraction they induce (pleochroïsm). Many systems are known to produce anomalous mixed crystals and their common behavior consists in a peculiar property of their host/guest interfaces:

i) a crystal-chemical affinity exists between certain planes of the matrix crystal and the planes of the crystalline species in which the impurity can crystallize;

ii) further, there is often a 3D affinity between the two species, the third parametric fit being the spacing of the lattice planes parallel in the two species

In Kern's opinion [5], one can imagine this growth mode as an epitaxial insertion of a crystal species in another one, favored by the advancing steps of the matrix crystal which should be able to bury the layers (of the same thickness) of the guest adsorbed phase.

Experimentally, an anomalous mixed crystal can form in a growth medium in which the impurity concentration might be much lower than its equilibrium concentration $C_{3\infty}$ (with respect to an infinite crystal). Kleber [6] proposed a mechanism to explain the formation of the anomalous mixed crystals. As a first step, a 2D adsorbed A-phase, ($A_2$), nucleates on a given face of the matrix crystal B, its concentration $C_A$ fulfilling the condition $C_{2\infty} < C_A < C_{3\infty}$. In other words, $C_A$ is sufficient to allow the 2D nucleation of the A phase on B, while is too low to allow the homogeneous nucleation of 3D crystals, ($A_3$). The relation ruling this nucleation is borrowed from the vapor/crystal system and reads:

$$C_{2\infty} / C_{3\infty} = \exp (\varphi_{AA} - \varphi_{AB})/k_B T \qquad (1a)$$

where $\varphi_{AA}$ represents (within the Kossel crystal model) the lateral interaction between two growth units of the A crystal and $\varphi_{AB}$ is the interaction between a growth unit of the A crystal and the matrix B. According to equation (1a) one can see that, if $\varphi_{AA} < \varphi_{AB}$ , then the $A_2$ phase is stable even if its corresponding $A_3$ phase does not form (see Mutaftschiev's and Kern's lectures). In other words, a 2D-phase ($A_2$) can form on a crystal B, even if the surrounding medium is unsaturated with respect to its bulk phase $A_3$.

Going from the interactions $\varphi_{AA}$ and $\varphi_{AB}$ to the specific surface energies (at zero Kelvin) and remembering the Dupré's relation ruling the host/guest interface:

$$\gamma_{AB} = \gamma_A + \gamma_B - \beta_{adh}^{AB} \qquad (1b)$$

equation (1a) transforms to: $\gamma_B > \gamma_A + \gamma_{AB}$ (1c)

where $\gamma_A$ and $\gamma_B$ , stand for the specific surface energies of the phase A and B , while $\gamma_{AB}$ and $\beta_{adh}^{AB}$ represent the excess energy of the interface AB and the specific adhesion energy between A and B, respectively [7].

Beyond the interesting energetic relationships ruling the formation of the anomalous mixed crystals, it should be worth recollecting the experimental evidences of this peculiar phenomenon. This will be done comparing the cases where the 2D epitaxial layers are only adsorbed on the growing face of the guest crystal with those where the foreign ordered adsorption is followed by the absorption in the growing crystal.

Since 1925 Gaubert put forward the idea that "… either the habit change of crystals or the oriented growth of a crystal A on a crystal B should be two phenomena generated by the same cause". Bunn [8] and Royer [9] tried to verify this hypothesis by crystallizing a certain number of substances with simple and well known structures. Royer showed that a new face can appear on a crystal (this is the habit change) when a lattice coincidence can be found between the 2D cell of the new face and the 2D cell of a face of the impurity: this represents a condition for epitaxy and then the habit change can be attributed to the epitaxy between the impurity (seen as a crystal) and the new face so obtained. The following example gives evidence of the inspired guess by Gaubert and Royer.

When growing from pure aqueous solution, many crystal species of the NaCl fcc-lattice type usually grows as a {100}-cube while the {111}-octahedron only appears (Fig.1) on the morphology of some of them, within a narrow range of supersaturation values [10]. It has been also demonstrated (experimentally and theoretically) that this habit change is only due to a kinetic effect and does not depend on the equilibrium shape of NaCl in pure aqueous solution [11a,b].

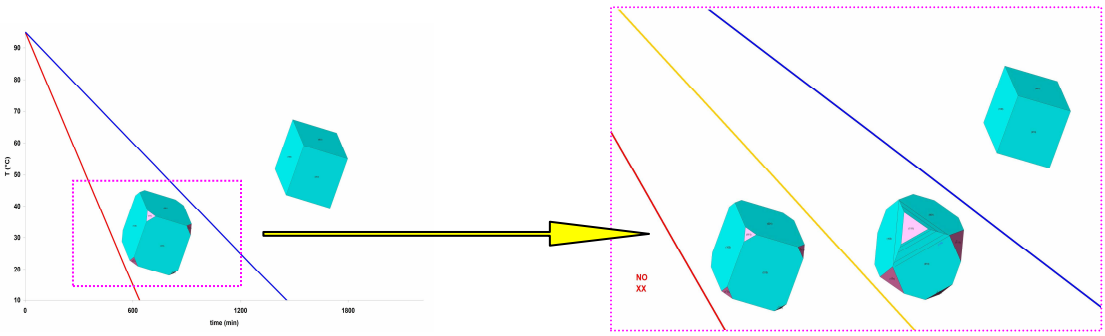


Fig.1a)- Morphology of NaCl crystals grown from pure aqueous solutions in a closed system according to different T gradients (T vs t diagram). Initial $T_{sat}$ and final $T_{cryst}$ are 95 and -5°C, respectively. Only cubes are observed when the gradient is lower than 3.5°C/h. Cube and octahedron coexist when the gradient lies in between 3.5 and 8°C/h. For gradients higher than 8°C/h no crystals have been observed. b)- Enlarged view of the intermediate zone, the mid-line corresponding to the slope of 4°C/h. Second generation crystals (larger) are composed by {100} and {111} forms, while in larger crystals (first generation) only {100} form survives to the kinetic competition.

On the other hand, evidence exists of the morphological change {100} → {110} or {100} → {111} due to the adsorption of specific impurities ( both inorganic and organic) on the NaCl surfaces, as illustrated in the lectures by R. Kern. Here we will confine our attention to a limited number of case studies, in order to outline the effects arising from the differences between the case of an ordered 2D-adsorption (2D-epitaxy) and that in which the coincidences between the growing substrate and the adsorbed impurity are not only governed by the 2D-epitaxy but extend to a three dimensional lattice.

## The first case

**Impurity adsorption ordered as a 2D lattice: 2D epitaxy between the impurity and the growing face** ⇒ **no fit between the thickness of impurity layers and the substrate** ⇒ **no impurity absorption in the growing face**

It is well known that NaCl shows a morphology built by the {100} and the prevailing {111} form, when growing from $CdCl_2$ doped aqueous solution [12].Here we will deal with the different interpretations that have been attempted to explain this morphology change:

***a)*** The impurity $CdCl_2$ crystallizes in a rhombohedral structure (S.G. $R\bar{3}m$ ; $a_0$= 3.85 Å, $c_0$= 17.46 Å) and the allowed thickness of its growth {00.1} form corresponds to the slice $d_{00.3}$ = 5.8266 Å containing three PBCs running along the three directions <100>. Then, the (00.1) face of $CdCl_2$ has a flat (F) character.

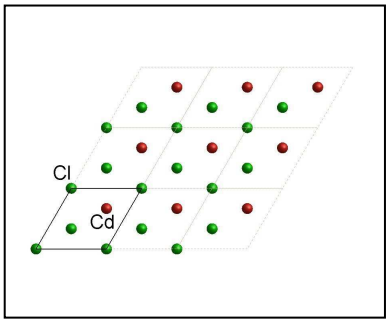


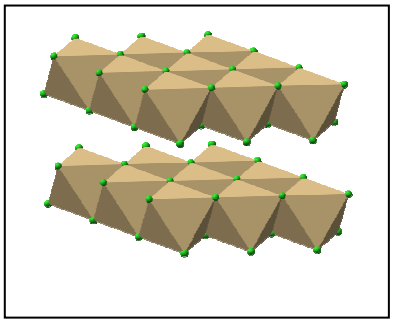

Fig.2 ( left ) The [001] view of $d_{00.3}$ layer of the $CdCl_2$ structure.
(right) The octahedral coordination of the Cd atoms within parallel $d_{00.3}$ layers is also drawn.

The reconstructed (111)-NaCl face is stable but cannot belong to the equilibrium shape of the crystal in pure aqueous solution, since its specific surface energy is too high, as mentioned above. Starting from the Royer's hypothesis, Hartman [12] imagined that a 2D (00.1) layer of $CdCl_2$ can form a good epitaxy with the (111)-NaCl face, as follows from the coincidences between the triangular 2D lattices of both crystals:

$$|[110]|_{NaCl} = 7.976 \text{ Å} \; ; \quad 2\times |[100]|_{CdCl2} = 7.70 \text{ Å} \quad \rightarrow \; \Delta = -3.46 \; \%$$

Concerning the bonds formed at the epitaxial interface, a layer of Cl atoms belongs both to the crystal-substrate and to the adsorbed $CdCl_2$ slice, the bonds formed between these Cl atoms and Cd atoms being considered as adsorption bonds. Further, the adsorbed layer is rendered stable by its lateral Cd-Cl bonds (Fig.3).

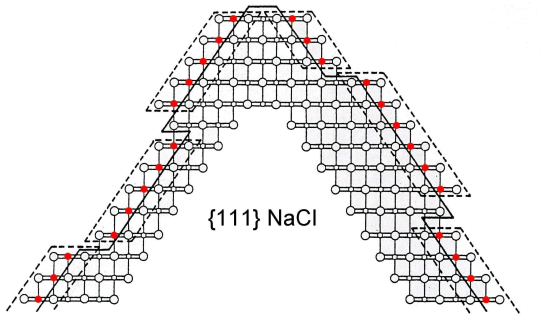


Fig.3 [110] projection of the NaCl structure. The profiles of the {111} NaCl form are drawn along with the adsorbed $CdCl_2$-layers, represented within the dashed lines (Cd ions in red). The two outmost $Cl^-$ layers belong both to the adsorbed phase and to the underlying (111) faces, whose structure is made by alternating Na+ and $Cl^-$ planes

According to this model, the $CdCl_2$ impurity is adsorbed as an ordered phase and:

- on one hand it lowers the specific surface energy of the (111) face of the NaCl crystal which probably enters the equilibrium shape of the crystal in the doped solution;
- on the other hand it lowers the growth kinetics of the (111) face as well, since the percentage of fresh (111) NaCl surface is surely reduced by the $CdCl_2$ adsorbed 2D islands

Finally, Hartman observed that there is not compatibility between the elementary layers of thickness $d_{111}^{NaCl}$ =3.256 Å and $d_{00.3}^{CdCl2}$ =5.8266 Å, respectively. As a matter of fact :

$$2\times d_{111}^{NaCl} = 6.512 \text{ Å} \; ; \; d_{00.3}^{CdCl2} = 5.8266 \text{ Å} \quad \rightarrow \; \Delta = -10.52 \; \%$$

represents a discrepancy too high in order the $CdCl_2$ adsorbed layer to be buried in the growing (111) NaCl face and then to allow the formation of anomalous mixed crystals.

***b)*** - $CdCl_2$ crystallizes, as a mixed salt of composition $CdCl_2 \cdot 2\,NaCl \cdot 3H_2O$ ( S.G. $R\bar{3}m$ ; $a_0$= 7.89 Å, $c_0$= 26.52 Å ), on the {111}-NaCl faces. This was not only a hypothesis, but was proved by Boistelle et al. [13] who observed a 3D epitaxy between the {111}-NaCl faces and the {00.1} faces of the mixed salt. The 2D-lattice coincidence at the epitaxial interface results to be even better than that calculated in the just mentioned case:

$$|[110]|_{NaCl} = 7.976 \text{ Å} \; ; \quad |[100]|_{mixed\ salt} = 7.89 \text{ Å} \quad \rightarrow \; \Delta = -1.08 \; \%$$

Hence, the idea of the habit change due to the action of a specific impurity adsorbed as an epi-layer is reinforced. Concerning the possibility of the formation of an anomalous mixed crystal, the compatibility between the allowed layers of thickness $d_{111}^{NaCl}$ =3.256 Å and

$d_{00.6}^{mixed-salt}$ = 4.42 Å is even worst that that calculated in the previous case. Actually, the difference in the layer thickness increases, for the NaCl/mixed salt couple, to Δ = +35.75 %.

## The second case

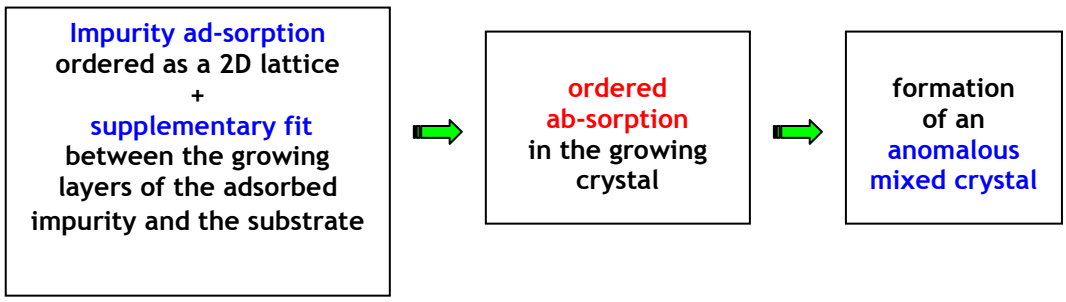


### a) - Calcite ($CaCO_3$) crystallizing in the presence of $Li^+$ ions

#### *a.1) - The historical background*

The influence of $Li^+$ ions on the crystal morphology of calcite became a matter of some interest twenty years ago, when: i)- Rajam and Mann [14] found that the {00.1} platy pinacoid was added to the classic {10.4} cleavage rhombohedron in $Li^+$ doped aqueous solutions; ii)- Nefyodova et al. [15] confirmed that {10.4} shaped seeds transform into crystals dominated by the {00.1} form in $Li^+$ bearing hydrothermal solutions. IR spectra and evaluation of the $Li^+$ segregation energy on the {00.1} form suggested that $Li^+$ cannot be absorbed within the growing calcite, but only randomly adsorbed in lattice and not interstitial sites on the {00.1} surfaces, so slowing down their advancement rate. No interpretation was given, at that time, on the growth mechanisms ruling this unusual morphological change (from kinked -K to flat -F character ) of the {00.1} form.

#### *a.2) - The "morphodrome" ($CaCO_3$ , $Li^+$ ). The {00.1}, {01.8} and {10.4} forms affected by the adsorption of $Li^+$ ions.*

As introduced in the Kern's lectures, a practical way of representing the morphological changes of a crystal species in the presence of a variable amount of an impurity, is to draw a *morphodrome*, i.e. a Cartesian diagram with the impurity concentration ($C_i$) on the abscissa and the supersaturation (β) with respect to the growing crystal on the ordinate axis. In this way, the occurrence domain of the different morphologies can be drawn in a 2D space. Fig.4 shows that, when $Li^+$ ions are added to the

pure calcite supersaturated aqueous solutions, the {00.1} form and the vicinal {01.1} rhombohedron enter enriching the growth morphology of bulky crystals which were built up by the sole {10.4} form when growing from pure solutions (under the same β value and $[Ca^{2+}]/[CO_3^{2-}]$ ratio). The importance of the {00.1}form increases when crystals nucleate and grow, in a steady state, in the presence of increasing amounts of lithium [16]. Then, the crystal habit becomes more and more {00.1} platy starting from an initial $[Li^{+}]/[Ca^{2+}]$ ionic concentration ratio equal to 0.01.

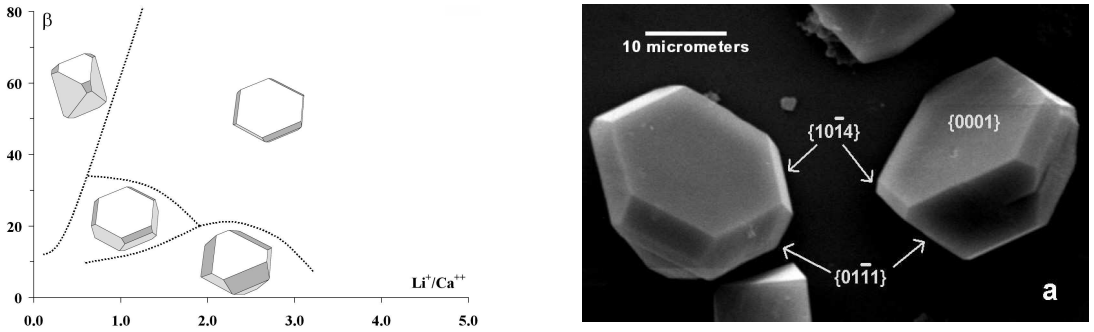


Fig. 4) Morphodrome of calcite crystals nucleated under varying initial $[Li^{+}]/[Ca^{2+}]$ concentration ratios and supersaturations. Different domains are associated to the most frequent observed habit.

From SEM and AFM observations it comes out that the {00.1} form shows layered surfaces within a wide range of supersaturations. A general ex-situ overview of crystals obtained at moderate $\beta$ values ($4 < \beta < 37$) indicates that the {00.1} surfaces are populated by pseudo-hexagonal growth hillocks built by more or less periodic sequence of terraces and macrosteps (Fig.5a,b). Their mean thickness varies in between 5 and 35 nm while the hillocks slope increases from 1° to 6.5° with increasing supersaturation. Hence it can be said that the kinetic behavior of {00.1} form is that of a F-form, independently of the step origin ( 2D nucleation or spiral growth). Moreover, from a deeper analysis of the profile of the terraces lying in between two successive macrosteps, it turns out that the terrace surfaces are not atomically flat. On the contrary, they are slowly wavy and populated by small cobbles whose height does not exceed a few nanometers ( Fig.5c). These cobbles behave as true obstacles for the spreading of the $d_{00.1}$ layers which slow down their advancement rate; this, in turn, generates the step bunching which is responsible of the macrostep occurrence.

Nevertheless, at low $\beta$ values, the {00.1} form really behaves as a F form. But, as much as the supersaturation increases, both height and size of the terrace cobbles increases too, so slowing down the macrosteps velocity.

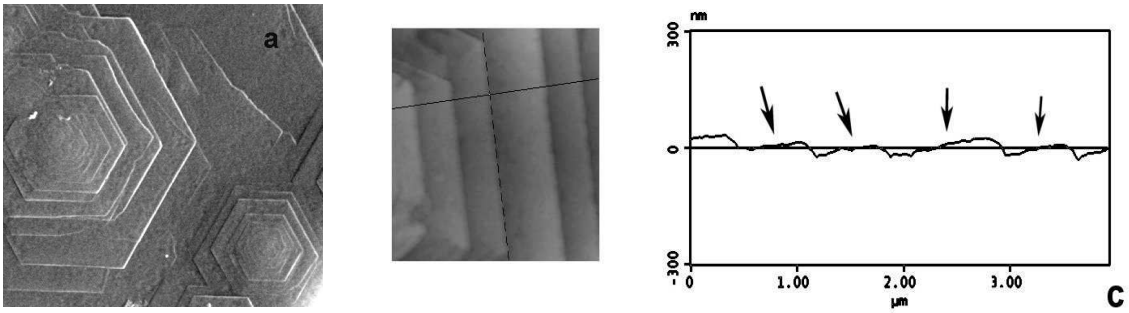


**Fig.5 S**urface structure of the {00.1} calcite form grown in the presence of $Li^+$ ions. a) SEM image showing pseudo-hexagonal growth hillocks. Macrosteps run along the <100> directions. b,c) AFM images of the profile of the terraces lying in between successive macrosteps showing small cobbles (arrows) and the wavy surface structure.

A critical situation occurs when, at high $\beta$ values, the cobbles height is able to compete with the macrosteps height, so hindering their flow. When this critical threshold is reached the inverse F $\rightarrow$ K transition takes place ( see Fig. 6) [17].

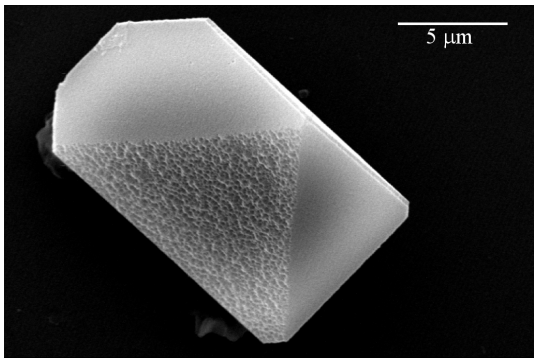


Fig.6 (left)- Calcite crystal nucleated and grown from $Li^+$ bearing solution at high supersaturation values ($\beta \geq 37$): the (00.1) faces begin to roughen. (bottom)- The slopes of the growth hillocks on the (00.1) faces.

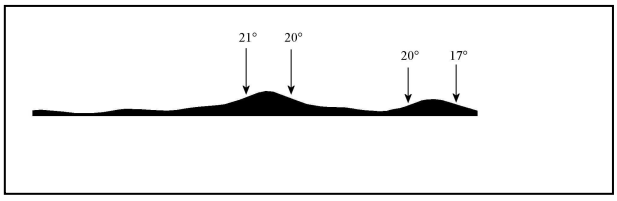


A clarifying phenomenon on the effects induced by lithium on growing calcite crystals is that observed on the {10.4} seeds, initially grown in pure medium and, successively, immersed in a lithium bearing supersaturated solution: the layer growth starting from {00.1} surfaces can also propagate on contiguous {10.4} form and generates new {01.8} surfaces. Figs.7a,b illustrate two successive stages of this covering effect on a {10.4} seed. Fig.7a shows that once lithium is added to the mother solution new layers start to stabilize the {00.1} form and then continue spreading on the adjacent free surfaces following the symmetry imposed by the triad axis. Fig.7b shows a further development of the covering which stopped just before the initial rhombohedron was entirely encompassed. It is worth also outlining that the $<\bar{4}41>$ edges of the original seed were replaced (during growth) by small rectangular shaped {01.8} surfaces [17]. Furthermore, the macroscopically stepped profile which characterizes the {01.8} surfaces of the natural samples ( Fig.8a ) does no longer appear in crystals grown in the presence of lithium; on

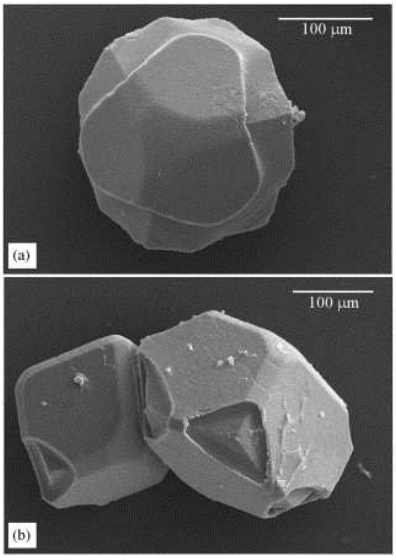


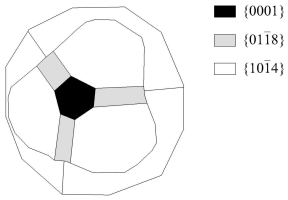


Fig7 a,b. The morphology changes induced on the {10.4} seeds of calcite by the presence of Li+ ions in the mother solution.
The new {00.1}and {01.8} surfaces are smoothed and look like those of the adjacent {10.4} flat form.

the contrary, the {01.8} surfaces illustrated in Fig.7 are smoothed and look like those of the adjacent {10.4} and {00.1} flat forms. We may invoke also in this case the role of the

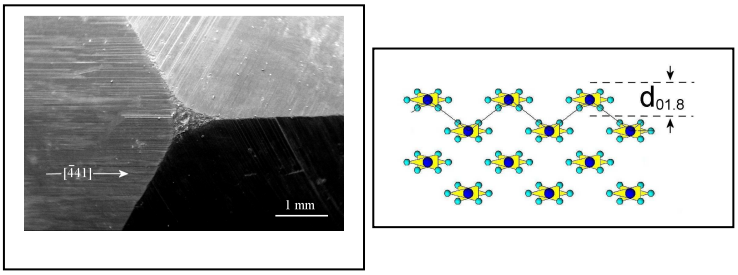


Fig.8(a) A [$\bar{4}$41] stepped profile characterizes the {01.8} surfaces of the natural calcite samples.(b)The character of this form is stepped because no bond exists between the [$\bar{4}$41] PBCs (up-down) within a $d_{018}$ slice.

2D epitaxy as the modifier of the {01.8} character (S → F). As a matter of fact, new lattice coincidences are found (Table 1) between $Li_2CO_3$ and calcite when comparing the 2D mesh of the {01.8} calcite form with those of the {001} and {100} forms of the $Li_2CO_3$ structure :

| | *Calcite* {01.8} *host* | *Zabuyelite* {001} *guest* | Misfit(%) | obliquity |
|---|---|---|---|---|
| 2D cell vectors and length (Å) | \|[010]\| = 4.989 | \|[010]\| = 4.972 | +0.34 | 0° |
| | 2/3×\|[010]\| = 25.66 | 3×\|[100]\| = 25.17 | +1.95 | |
| Layer thickness (Å) | $d_{01.8}$ = 1.9125 | $d_{002}$ = 2.81229 | - 47.04 | |
| | *Calcite* {01.8} *host* | *Zabuyelite* {100} *guest* | | |
| 2D cell vectors and length (Å) | \|[010]\| = 4.989 | \|[010]\| = 4.972 | +0.34 | 0° |
| | 1/3×\|[48$\bar{1}$]\| = 12.83 | 2×\|[001]\| = 12.42 | +3.30 | |
| Layer thickness (Å) | 2×$d_{01.8}$ = 3.825 | $d_{200}$ = 3.79327 | +0.836 | |

Table 1. Lattice coincidences at the $\{01.8\}_{calcite}/\{001\}_{zabuyelite}$ and$\{01.8\}_{calcite}/\{100\}_{zabuyelite}$ interfaces.

From the Table 1 one can see the excellent 2D-coincidences between both the $\{001\}_{zab}$ and $\{100\}_{zab}$ forms and the $\{01.8\}_{calcite}$. It should be also remembered that $\{001\}_{zab}$ is a F form while $\{100\}_{zab}$ is a S one, as it ensues from the PBC analysis; further, $\{001\}_{zab}$ is the most important form entering the equilibrium shape of the crystal, whilst the $\{100\}_{zab}$ is excluded owing to the high value of its surface energy [18].Then $\{001\}_{zab}$ seems to be favored to make epi-layers which should change the character (S $\rightarrow$ F) of the $\{01.8\}_{calcite}$. Concerning the fit of $d_{002}$ and $d_{200}$ thickness (zabuyelite) with the $d_{01.8}$ (calcite), the related contributions to the formation of anomalous mixed crystals will be discussed later on.
Aiming at explaining the $Li^+$ effect on the appearance of both the new $\{00.1\}$ and $\{01.8\}$ forms of calcite, we will adopt the interpretative path proposed by the Kern's school. At first, we will reasonably concentrate our attention on the epitaxy model (geometric and structural) of the adsorbed (001)-$Li_2CO_3$ layers on the (00.1)-$CaCO_3$ substrate.

### *a.3)- The epitaxial model of the interface between (001)-$Li_2CO_3$ (zabuyelite) and the substrate (00.1)-$CaCO_3$(calcite).*

The space group of calcite is $R\bar{3}c$ and its parameters (hexagonal frame), are: $a_o$= 4.989 Å, and $c_o$= 17.06 Å, while $Li_2CO_3$, at ambient conditions, is monoclinic (C2/c), with $a_o$= 8.39 Å, $b_o$= 5.00 Å, $c_o$= 6.21 Å, $\beta$ = 114.50°. Comparing these structures, viewed along their [010] directions, one can see that their geometrical misfits are very low (Table 2).

| | Calcite$\{00.1\}$host | Zabuyelite $\{001\}$ guest | Misfit(%) | obliquity |
|---|---|---|---|---|
| 2D cell vectors and length (Å) | $\|[210]\|$= 8.64 | $\|[100]\|$= 8.359 | +3.3 | 0° |
| | $\|[010]\|$= 4.989 | $\|[010]\|$= 4.972 | +0.34 | |
| Layer thickness (Å) | $d_{00.6}$ = 2.843 | $d_{002}$ = 2.812 | +1.1 | |

Table 2. Lattice coincidences at the $\{00.1\}_{calcite}/\{001\}_{zabuyelite}$ interface.

a) - This means that the *geometrical conditions* for epitaxy between the (00.1) face of calcite crystal and the $d_{002}$ layers of lithium carbonate are largely fulfilled.
b) - Concerning the *structure of the epitaxial $d_{002}$ layer of $Li_2CO_3$* it is worth outlining that the outmost $Li^+$ ions, which should face the outmost (00.1) layer of calcite, form a perfect 2D hexagonal lattice, as it ensues from a projection of the $Li_2CO_3$ structure normal to the 001 plane. Entering into details, $Li^+$ ions lie in the origin of the 2D space group *p6m*, the lattice vector corresponding to $b_o^{Li_2CO_3}$ =4.972 Å. This lattice coincides (misfit of 0.2%) with that built by the vacant sites resulting from the second restructured layer of calcite (00.1).

In other words and remembering the reconstructed {111} NaCl surfaces [19] ( see Bruno's lectures in this Book) one can say that, if the outmost calcite layer contains only the 25% of $CO_3^{2-}$ ions, in the following one the 75% of available sites will be occupied by $Ca^{2+}$ ions while the $Li^+$ ions could fill the remaining ones. Hence a $d_{002}$ layer of $Li_2CO_3$ can be adsorbed on the $(00.1)_{calcite}$ face. Within this $d_{002}$ layer, three PBC's develop: the strongest one is the [010] PBC, while the two others are the <110> PBC's [20]. The adsorbed layer behaves as a 2D crystal which imposes its own PBC's to the underlying face [21]. In our peculiar case the strong [010] PBC of the $Li_2CO_3$ adsorbed layer runs along the same direction of the [010] steps we observed and described above; moreover, owing to the three-fold symmetry of the (00.1) face of calcite, the adsorbed impurity shall impose three strong PBC's to the face which, in turn, transforms its character from kinked to flat (K→F transition).

### *a.4) - The third condition to be fulfilled to get an "anomalous Calcite/Zabuyelite mixed crystal"*

Another geometric concordance, even not necessary for the epitaxy to occur, is that found between the thickness of the epitaxial $d_{00l}$ layers of both structures. From systematic extinction rules, the thicknesses allowed are $d_{00.6}$ = 2.843 Å and $d_{002}$ = 2.812 Å for calcite and $Li_2CO_3$, respectively: then, the relative misfit does not reach +1.1%. Thus, the parametric coincidences (in the three space directions) between the absorbing and the adsorbing crystal phases, should be fulfilled in order an *anomalous Calcite/Zabuyelite mixed crystal* to be formed. To verify this hypothesis, i.e. to investigate whether and how lithium can be absorbed into the calcite lattice, integrated characterization techniques, such as ICP, SEM, AFM, XRPD, cathodoluminescence (CL) and EPR, have been applied to a wide population of calcite single crystals grown both from solution and gels [22].

#### *a.4.1.) - CL measurements*

These measurements take advantage of the incompatibility between the structure of Li-carbonate and the $Mn^{2+}$ ions (present as impurity in the gel matrix) captured in it. Further, it is well known that $Mn^{2+}$ capture in carbonates shows marked CL effect since Mn-depleted sectors are frankly darker than the richer ones. From CL measurements one can argue the existence of irregular stacking sequences of $Mn^{2+}$-rich and $Mn^{2+}$-depleted layers within the {00.1} growth sectors of calcite and this proves, indirectly, that *lithium has been buried during growth* in the $Mn^{2+}$ -depleted layers

#### *a.4.2.) – XRPD measurements*

The 10.4 is the highest diffraction peak of calcite. In pure $CaCO_3$ samples, the highest intensity elementary curve among the ones resulting from the decomposition (Fig.9a ), is

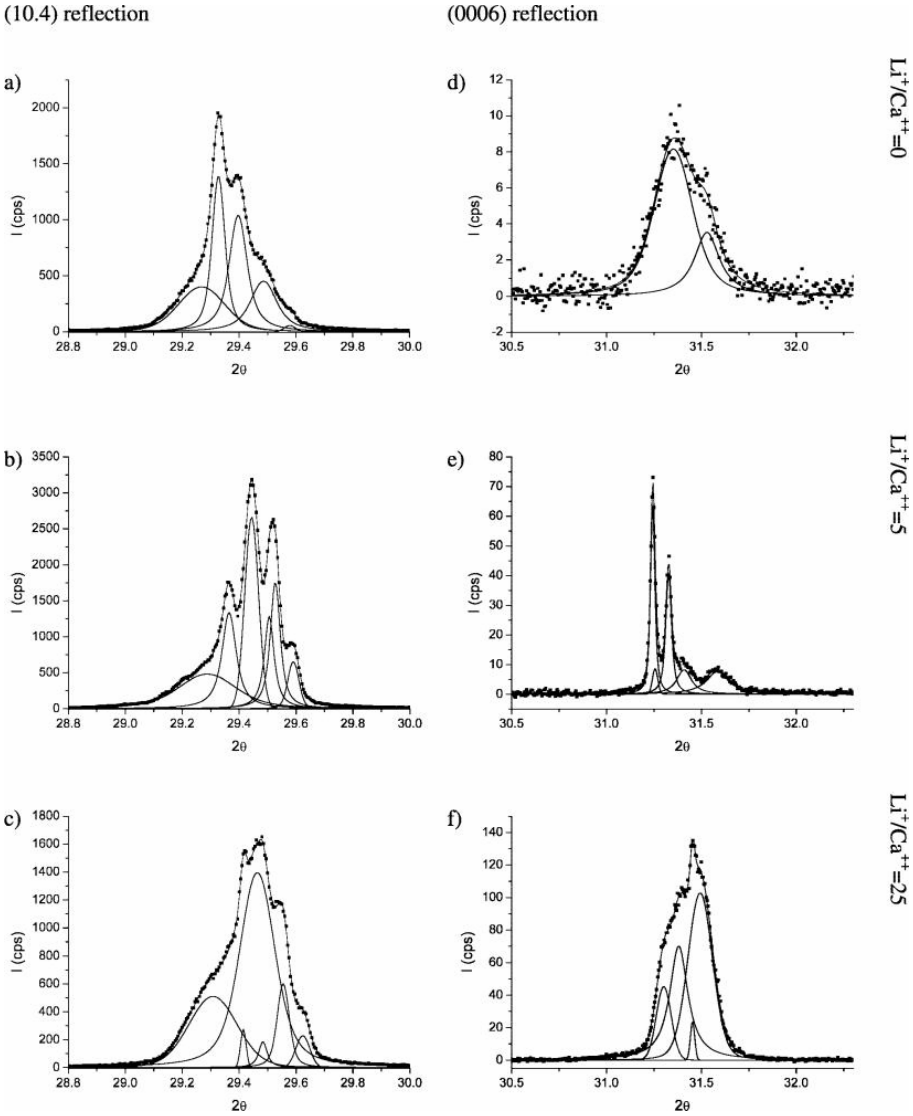


Fig.9 In pure $CaCO_3$ samples (a) the highest elementary curve is located at $d_{10.4}$ = 3.043 Å. With increasing $Li^+$ amount in the growth solution, the maximum progressively shifts toward lower spacing, that is at $d_{10.4}$ = 3.031 Å and $d_{10.4}$ = 3.028 Å when $Li^+/Ca^{2+}$ = 5 and 25, respectively ( b,c ). This is due to the overlapping of the $Li_2CO_3$ layers of thickness $d_{111}$ = 3.0311 Å in the {10.4 } growth sectors of calcite. An analogous behavior is illustrated for the 00.6 peak of calcite (d-f) which is strongly affected by the overlapping of the absorbed $Li_2CO_3$ crystal layers of thickness $d_{00.2}$

located at $d_{10.4}$=3.043 Å. With increasing $Li^+$ amount in the growth solution, the maximum intensity progressively shifts toward lower interplanar spacing, that is at $d_{10.4}$ = 3.031 Å and $d_{10.4}$ = 3.028 Å when $Li^+/Ca^{2+}$ = 5 and 25, respectively (Fig.9b,c ). Hence the dispersion of the maximum is not symmetric around the averaged value of the peak $<d_{10.4}>$ = 3.035 Å. It is worth noting that the $d_{111}$ reflection of pure $Li_2CO_3$ crystals occurs at $d_{111}$ = 3.0311 Å and that, consequently, the presence of mixed $CaCO_3$-$Li_2CO_3$ layers in the {10.4 } growth sectors of calcite should affect the position of the maximum corresponding to the $d_{10.4}$ peak.

As a matter of fact, a new relationship can be obtained at the $\{10.4\}_{calcite}/\{111\}_{zabuyelite}$ epitaxial interface, as illustrated in the following Table 3 and in Fig. 10.

| | Calcite {10.4 }host | Zabuyelite {111} guest | Misfit(%) | obliquity |
|---|---|---|---|---|
| 2D cell vectors and length (Å) | $1/3 \times \lvert[42\bar{1}]\rvert = 8.11$ | $\lvert[0\bar{1}1]\rvert = 7.9436$ | +2.09 | 2.34° |
| | $\lvert[020]\rvert = 9.9792$ | $\lvert[\bar{1}10]\rvert = 9.7266$ | +2.6 | |
| Layer thickness (Å) | $d_{10.4} = 3.043$ | $d_{111} = 3.0311$ | +0.39 | |

Table 3. Lattice coincidences at the $\{10.4\}_{calcite}/\{111\}_{zabuyelite}$ interface.

From Fig.10 it follows that an elementary $d_{111}^{zabuyelite}$ slice can only grow through 1D-nucleation of uncorrelated $[\bar{1}10]$ chains and then their adsorption on the $\{10.4\}$ form of

Fig.10

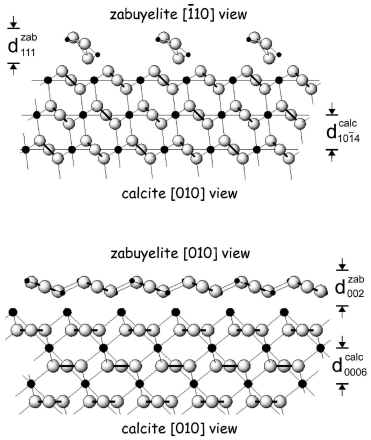


Projections of calcite (hexagonal frame) and $Li_2CO_3$ zabuyelite (monoclinic). Large and small spheres represent calcium and lithium atoms, respectively.
(top)-the structure of the $\{10.4\}_{calcite}/\{111\}_{zabuyelite}$ interface: the {111}form of zabuyelite is a stepped one, since any bond can be found among adjacent $[\bar{1}10]$ PBCs of zabuyelite within a $d_{111}$ slice
(bottom)-the structure of the $\{00.1\}_{calcite}/\{001\}_{zabuyelite}$ interface. It is worth noting that the thickness of the elementary layers are near the same in both structures, $d_{00.6}$ (calcite) being practically equal to $d_{002}$ ($Li_2CO_3$)

calcite is less favored with respect to that of zabuyelite 2D-nuclei ( of thickness $d_{002}$ ) on the $\{00.1\}_{calcite}$ pinacoid. Nevertheless, if the adsorption occurs, 1D zabuyelite chains can be easily buried within the $\{10.4\}$ growth sectors by new freshly created calcite layers, owing to the quasi perfect coincidence between the layers thicknesses of the two crystals. This seems to be the most reasonable way of explaining the progressive shift of the highest intensity component of the 10.4 diffraction peak ( and hence of the lowering of the $d_{10.4}$ value) of our crystals, with the increasing amount of lithium in the growth solution.

The 00.6 diffraction peak is an important one, its intensity being 73/100 of the main 10.4 reference peak. Its decomposition (Fig.9d,e,f) yields a unique averaged value $<d_{00.6}>$ = 2.8469 Å, corresponding to $c_0$ =17.080 Å which is very close to the value of 17.073 Å calculated from the overall XRPD spectra in non-lithium bearing calcite crystals. But, when the $Li^+$ amount increases in the growth solution, the peak shape dramatically changes and the spacing coming out from the decomposition spreads over a $\Delta d_{00.6}$ interval of 0.169 Å, resulting in a fairly symmetrical peak dispersion around $<d_{00.6}>$.

All this further proves that:

i) - $Li^+$ ions are absorbed in calcite taking the structure of zabuyelite layers and mainly locate in the {00.1} growth sectors of calcite, so perturbing the ordered stacking of its $d_{00.6}$ layers. This should induce zones of small compression and distension that are reflected in the dispersion of the cell parameter $c_0$ from 16.985 to 17.154 Å (around the value of 17.073 Å measured in pure calcite crystals).

ii) - Another growth sector affected by lithium absorption, even if to a lesser extent, is that of the {10.4} rhombohedron. This is not surprising, since we already observed that pure calcite seeds, originally limited only by the {10.4} form, are encompassed by thick growth layers which start to grow from the new generated {00.1} form, when lithium is added to the growth solution (see the preceding Fig.7).

***a.5 )- A first tentative conclusion***

Summing up:

i)- The incorporation of lithium into calcite does not randomly occur, but needs an epitaxial mediation. This means that 2D coincidence lattices between lithium and calcium carbonates ( so different in symmetry, but so close as concerns the structural packing ) are not confined to a geometrical meaning but represent the necessary condition for lithium to be incorporated through the epitaxial adsorption of PBCs (1D) or islands (2D).

ii)- Adsorption is followed by the absorption into growing calcite crystals owing to the equality between the thickness of the elementary layers (that of the adsorbed one and that of the underlying reactive substrate).

iii)- Thus, the anomalous mixed crystal originates thanks to a selective mechanism, since the probability of lithium entering the calcite lattice varies from {00.1} to {10.4} growth sectors, the first one being largely favored, as it ensues from the contrast shown by cathodoluminescence imaging.

iv) – On this ground, the anomalous calcite/zabuyelite mixed crystals, in the sense of Johnsen and Neuhaus, are not homogeneous, as proved by the cathodoluminescence and the different spreading of the 00.1 and 10.4 XRPD peaks.

**b) - Halite (NaCl) crystallizing in the presence of formamide ($H\text{-}CO\text{-}NH_2$)**

***b.1) - {100} → {111} morphological change in NaCl crystals growing from aqueous solutions in the presence of formamide. The literature data.***

The early work on this topic dates back to Gille and Spangenberg [23] who found the {100} → {111} habit change in NaCl crystals obtained from evaporating aqueous solutions in the presence of formamide. Much later, Bienfait et al. [10] determined the stability

domains of the cube and the octahedron (morphodrome) as a function of two parameters: the initial supersaturation of the solution, with respect to NaCl, and the formamide concentration in solution (Fig.11a). It is known, since the papers by the Kern's group on this topics, that formamide exerts on NaCl crystals an influence similar to that obtained with urea [24], i.e.: formamide lowers the critical supersaturation value ($\beta_{cr}$), at which the transition {100}→ {111} occurs, with respect to that measured in pure water solution. As a matter of fact, the {100}→ {111} transition was observed at $\beta_{cr}$ = 1.004 in pure formamide, while the corresponding value, in pure water, reaches $\beta_{cr}$ = 1.23. This was interpreted by considering that both urea and formamide have a similar steric hindrance that allows them to occupy the vacant sites, on the octopolar reconstructed {111} form of NaCl, where the surface electric field reaches its highest value. The stability of the {111}-NaCl form should further increase (with respect to that obtained in pure aqueous solution) since the dipole moment of urea and formamide is definitely higher than that of the water molecule.

Recently, Radenović et al. [25-29] confirmed these results by evaporating (at T=25°C) NaCl aqueous solutions containing up to 30% formamide, and outlined that its

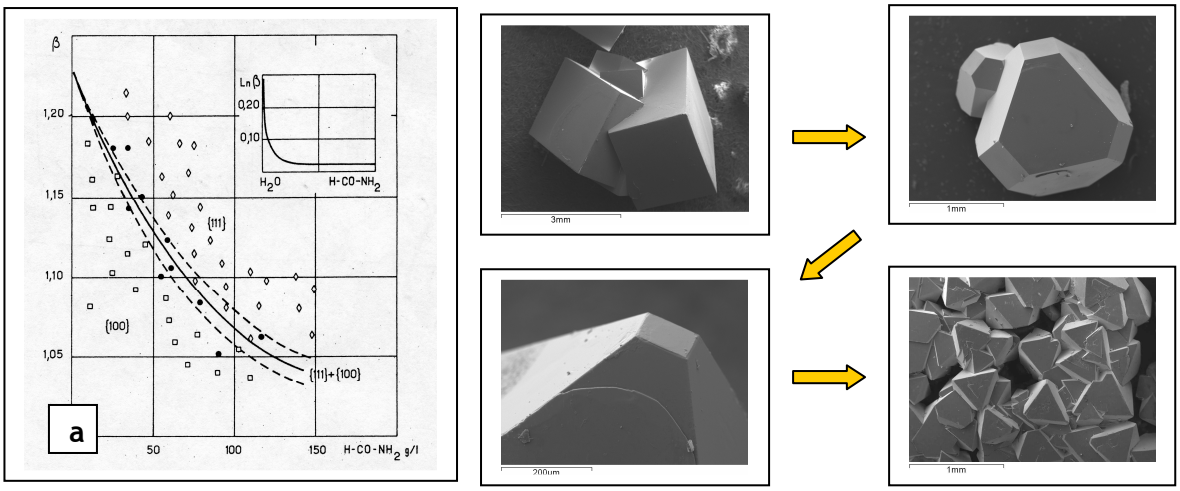


Fig.11 a)- Morphodrome of NaCl crystals grown from aqueous solutions in the presence of formamide (concentrations on the x-axis); on the y-axis, the initial supersaturation of the solution with respect to NaCl (from [10]). In the inset: the morphodrome represents the situation comprised between the limiting cases of pure water and pure formamide solutions. (b) {100} form from pure aqueous solution; c) {100}+{111} forms from aqueous solution containing 20% of formamide, obtained by evaporation at 25°C; d) a macrostep spreading on the {111} form (detail of the preceding case); e) uniqueness of the {111} form, grown from pure formamide solution.

presence enhances the quality of NaCl crystals, since the number of fluid inclusions sharply decreases with respect to those found after growth from pure aqueous solutions. Moreover, determining the structure of the {111} NaCl-liquid interface through a surface X-ray diffraction (SRXD) and using ultra-thin water or formamide layers, this research team showed that the crystal surface is smooth at an atomic level and is not reconstructed.

These results revealed small differences in surface structure between water or formamide liquid layers which, nevertheless, lead to dramatic differences in crystal morphology. From SRXD measurements it was also determined that {111} surfaces are $Na^+$ terminated for both environmental conditions and that 0.25–0.5 of a monolayer of laterally disordered $Cl^-$ ions is located on top of a fully ordered $Na^+$ crystal surface with occupancy 0.75–1.0. This means that polar surfaces are stabilized by an electrochemical double layer.
A further consideration has been proposed by the Vlieg's group to detail the influence of formamide on the NaCl morphological change: they noticed that for alkali halide crystals grown from saturated formamide solutions, the appearance of the {111} form is strictly related to unit cell size. Octahedrons appear starting from NaF crystals (unit cell size = 4.62 Å) to KCl with a unit cell of 6.28 Å. All alkali halide crystals with dimensions outside this range of unit cells crystallize as cubes and this confirmed that, apart from dipole-ion interaction, also the volume and the shape of the molecules are important for the stabilization of the {111} alkali halide surfaces by ad-sorption.

Thinking that such a dramatic change of morphology may be hardly interpreted in the light of the sole interactions between isolated molecules and the crystal surface, we investigated the structure of formamide in order to find if any cooperative effect (such as the epitaxial relationships) can set up between the crystal structures of NaCl (host phase) and formamide (guest phase). To do this, we started from the structure of formamide.

### *b.2) - The structure of formamide*

At the temperature of 223 K, formamide is monoclinic (S.G. $P2_1/n$), its lattice parameters being: $a_0$=3.69 Å, $b_0$=9.18 Å, $c_0$=6.87 Å, $\beta$=98°. Its structure [30-32] can be viewed as made by adjacent sheets of molecules which are parallel to the 101 plane and separated by the distance $d_{101}$ which reaches the value of 3.09 Å at 0°C, just below the melting point (+2°C) at room pressure (see table 4). Within the sheets, pairs of molecules associate to form almost coplanar dimers. Puckering of the sheets results from the tilt of the bimolecular units relative to one another. N-H···O bonds of two types cross-link the chains forming each sheet: H-bonds ($\alpha$), 2.93 Å nm long, link monomers to form dimers, while H-bonds ($\beta$), 2.88 Å nm long, link dimers together. In the light of the Hartman-Perdok theory, one can say that two PBCs run within the layers of thickness $d_{101}$: the PBC [010], developing along the screw $A_2$ axis through $\alpha$ -bonds and the PBC $[11\bar{1}]$ made by $\beta$-bonds. Remembering that no H-bonds can be found outside the $d_{101}$ layers, it is easy to consider the (101) formamide pinacoid as the most important F form of the crystal and then that the theoretical crystal habit ( at least from vapor phase) should be {101} platy. This is the main

reason why we chose the 101 plane as the best candidate for a hypothetical epitaxy between a $d_{101}$ layer of formamide and the growing NaCl-{111} form.

| | Host-NaCl {111} | Guest-formamide {101}♦ | misfit % | obliquity |
|---|---|---|---|---|
| 2D cell vectors (Å) | $\lvert[11\bar{2}]\rvert$ = 13.81 | 3/2 $\lvert$[010]$\rvert$ = 13.84959 | -0.286 | 0° |
| | $\lvert[1\bar{1}0]\rvert$ = 7.976 | $\lvert[10\bar{1}]\rvert$ = 8.16682 | -2.392 | |
| layer thickness (Å) | $d_{111}$ = 3.25 | $d_{101}$ = 3.0947 | + 4.778 | ----- |

**Table 4** Coincidences at the $\{111\}_{NaCl}/\{101\}_{formamide}$ interface. Structural data♦ are extrapolated at T= 0°C, from formamide structures determined at 90 [32], 108K [31] and 223 K [30], respectively.

From Table 4 one can be aware of a striking 2D-lattice coincidence that may set up both at the $\{111\}_{NaCl}/\{101\}_{formamide}$ interface and between the thickness of the elementary layers $d_{111}^{NaCl}$ and $d_{101}^{formamide}$. All that means that it is worth searching for prove the existence of NaCl/formamide anomalous mixed crystals.

### *b.3) - The {100} → {111} NaCl morphological change due to formamide ad-sorption and its selective ab-sorption in the bulk of the NaCl lattice*

Starting from the experience acquired in the formation of the calcite/zabuyelite anomalous mixed crystals, we did not confine our attention to the morphology of the NaCl crystals grown in the presence of formamide, but investigated also their bulk structure, in order to find if the adsorption → absorption mechanism would also occur in this new case. Fig.12 shows the XRPD spectra recorded on different populations of NaCl crystals obtained at different crystallization temperature ($T_c$) and from solutions containing different concentrations of formamide ($C_f$). Two main (2θ) intervals, corresponding to the $d_{111}$ and $d_{002}$ equidistances of the NaCl crystal are worthy of consideration.

#### (a) 27°≤ 2θ ≤ 28° → the $111_{(NaCl)}$ and the $101_{(formamide)}$ reflections

**$i_{(111)}$** A saturated ($T_s$=95°C) NaCl aqueous solution ($C_f$ =20%) was cooled, under a gradient of 20°/h, at = -5°C. XRPD spectra were carried out at T=-5°C as well, on a large population of un-grinded as grown {111} platy shaped crystals. Fig.12a,left side shows two diffraction peaks. The first one, at lower 2θ values, corresponds to the integrated $\lambda_{K\alpha 1}$ and

$\lambda_{K\alpha 2}$ contributions of the reflection $<d_{111}^{NaCl}>$=3.2593 Å. The second one, i.e. the low intensity peak at 2θ =27.695, *cannot be indexed as a NaCl reflection* but as the $d_{101}^{formamide}$ = 3.2209 Å (using the averaged $\lambda_{K\alpha 1,2}$ =1.54178 Å). This $d_{101}^{formamide}$ value is slightly higher (+4.07%) than the calculated one (3.0947 Å) by extrapolation of structural data of the pure formamide. This means that NaCl crystals were able to capture formamide in their bulk during growth (either through fluid inclusions or by absorption of ordered $d_{101}$ layers, or both). Since these spectra were obtained at T=-5°C, where formamide is necessarily crystallized, other measurements must be made at T ≥ +2°C, i.e. beyond its melting point. Therefore, all the experiments described in the following were performed by evaporating a solution ($T_{ev}$=30°C) and the corresponding XRPD spectra were carried out at T=+25°C.

**ii$_{(111)}$** NaCl crystals formed from a water/formamide solution($C_f$ =20%). Their morphology is made by dominating {100} and small {111} forms. The $111_{NaCl}$ peak is weakly

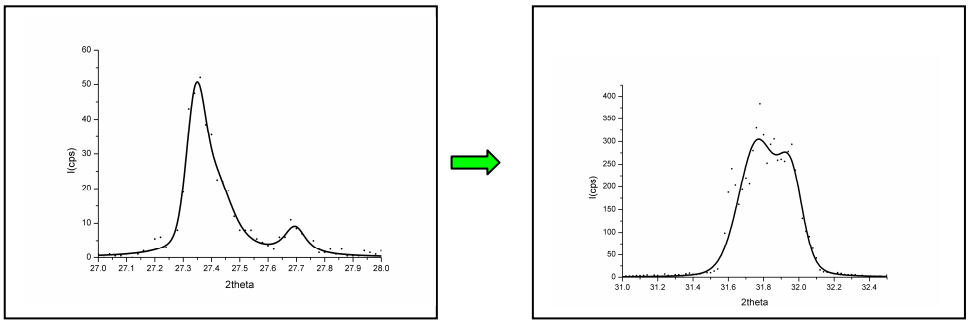


Fig.12a: XRPD spectra performed at T=-5°C on crystals obtained at $T_{cr}$ = -5°C from a saturated ($T_s$=95°C) NaCl aqueous solution ($C_f$ =20%) cooled under a gradient of 20°/h. Left side: 111 $_{NaCl}$ peak (lower angle) + 101 $_{formamide}$ peak (higher angle). Right side: 002 $_{NaCl}$ peak

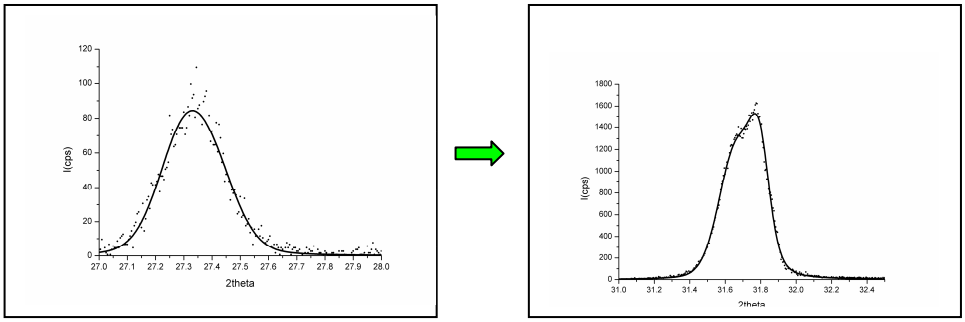


Fig.12b: XRPD spectra performed at T=25°C on crystals obtained by evaporation at $T_{cr}$ = 30°C from a NaCl aqueous solution (initial $C_f$ =20%). Left side: asymmetric 111 $_{NaCl}$ peak (lower angle). Right side: 002 $_{NaCl}$ peak

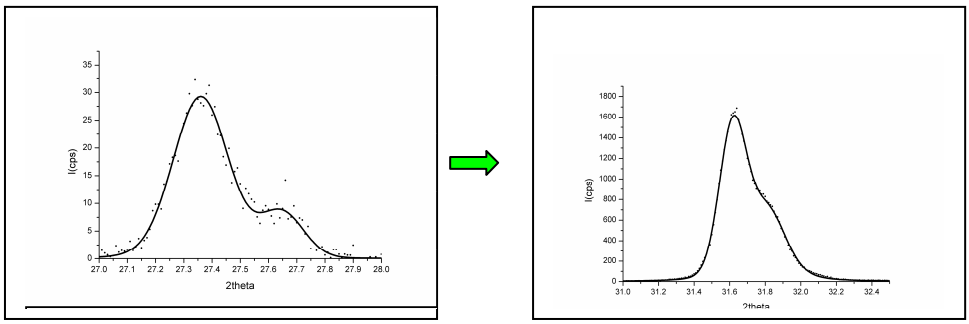


Fig.12c: XRPD spectra performed at T=25°C on crystals obtained by evaporation at $T_{cr}$ = 30°C from a NaCl aqueous solution (initial $C_f$ =60%). Left side: asymmetric 111 $_{NaCl}$ peak (lower angle). Right side: 002 $_{NaCl}$ peak

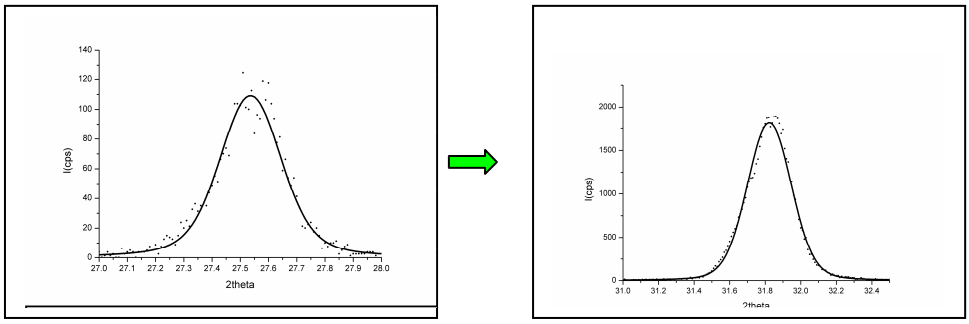


Fig.12d: XRPD spectra performed at T=25°C on crystals obtained by evaporation at $T_{cr}$ = 30°C from a NaCl pure formamide solution ($C_f$ =100%). Left side: 111 $_{NaCl}$ peak. Right side: 002 $_{NaCl}$ peak

asymmetric (due to the $\lambda_{K\alpha 1}$ and $\lambda_{K\alpha 2}$ components) and yields $<d_{111}^{NaCl}>$=3.2604 Å. No other peak occurs in the observed 2θ range. (Fig.12b,left side) The small increase (+0.033%) of the $d_{111}^{NaCl}$ value is not surprising, owing to the increased temperature of measurement (from -5 to +25°C). However, no *ad*-sorbed $d_{101}^{formamide}$ layers are found to be orderly *ab*-sorbed in the growing NaCl crystal.

**iii$_{(111)}$** NaCl crystals were obtained from a new water/formamide solution ($C_f$ =60%). Their morphology is now made by dominating {111} and small {100} forms. The full width at mean height (FWMH) of the 111$_{NaCl}$ peak ($<d_{111}^{NaCl}>$=3.2596 Å) increases with respect to the preceding case. A satellite peak occurs at 2θ =27.650 and corresponds to $d_{101}^{formamide}$ = 3.226 Å (Fig.12c,left side). Any effect of crystallization of formamide fluid inclusions must be excluded since both the crystallization and recording temperatures were largely higher than the melting point of formamide. Then, when the concentration of formamide

competes with that of water, the $d_{101}^{formamide}$ layers are not only epitaxially adsorbed on the $111_{NaCl}$ surface but also buried in the growing crystal.

**iv** $_{(111)}$ The just mentioned conclusion is spectacularly confirmed by NaCl crystals obtained from pure formamide solution. The only form is the {111} octahedron. XRPD spectra yielded *a unique and symmetric peak which locates in between the* $111_{NaCl}$ *and the* $101_{formamide}$ *peaks.*(Fig.12d,left side) Thus, as a first approximation, $d_{111\,NaCl}^{101\,formamide}$ = 3.2393 Å.

**(b) $31^\circ \leq 2\theta \leq 32.5^\circ \rightarrow$ the $002_{(NaCl)}$ reflection**

The behaviour of the $002_{(NaCl)}$ reflection is rather different with respect to the preceding one. In the $31^\circ \leq 2\theta \leq 32.5^\circ$ interval there is no risk of overlapping between the $002_{(NaCl)}$ peak and formamide reflections. Nevertheless both the $d_{002}^{NaCl}$ value and the corresponding peak profile are affected by the formamide layers absorbed in the crystal within the {111} growth sectors. In the following we will illustrate the behaviour of the $002_{(NaCl)}$ peak, analogous of the just described situations ($\mathbf{i}_{111}$, $\mathbf{ii}_{111}$, $iii_{111}$ and $iv_{111}$):

**i**$_{(002)}$ $C_f$ =20%; $T_{crystallization}$ = -5°C; XRPD spectra were performed at T=-5°C, as in **i**$_{(111)}$. A large peak is obtained, its complex profile being composed by three different contributions (Fig.12a,right side): a low angle component due to $d_{002}^{NaCl}$=2.827 Å, a medium angle component located at $d_{002}^{NaCl}$=2.8137 Å and a high angle component at $d_{002}^{NaCl}$=2.7974 Å. The averaged value of these spacing locates at $d_{002}^{NaCl}{}_{averaged}$ = 2.8127 Å which is – 0.35% lower that the corresponding value calculated from the reflection $<d_{111}^{NaCl}>$=3.2593 Å observed in $\mathbf{i}_{111}$. This is not surprising if one remembers that the {111} platy shape of the crystals obtained in this case favors the dispersion of the $d_{002}^{NaCl}$ spacing owing to the varying amount of formamide captured within the $d_{111}^{NaCl}$ layers in the +95°C $\rightarrow$ -5°C growth interval.

**ii**$_{(002)}$ $C_f$ =20%, $T_{ev}$ = 30°C $\rightarrow$ The 002 peak profile is asymmetric (Fig.12b,right side): from the lower angle component the averaged value ($\lambda_{K\alpha 1,2}$) results to be $<d_{001}>_{lower\ angle}$ = 5.6515 Å which only differs by –0.033% from the calculated $<d_{001}>$ = 5.6534 Å obtained from the measured $<d_{111}>$ =3.2604 Å (as it can be seen in $ii_{111}$). Further, the averaged value of the higher angle component of the asymmetric peak locates at $<d_{001}>_{higher\ angle}$ = 5.6288 Å, so showing that within the same crystal population there are two generations of $<d_{001}>$

equidistances, which are differently affected by the capture of $d_{101}$ ordered layers of formamide. In this case, the split of $<d_{001}>$ = ($<d_{001}>_{lower\ angle} - <d_{001}>_{higher\ angle}$) is 0.0227Å

**iii$_{(002)}$** $C_f$ =60%, $T_{ev}$ = 30°C → The 002 peak profile maintains asymmetric, but its shape changes, due to the displacement of its two components (Fig.12c,right side). From measurement: $<d_{001}>_{lower\ angle}$ = 5.6603 Å while $<d_{001}>_{higher\ angle}$ = 5.6262 Å → the split reaches 0.0341 Å .The variation in the splitting of the two components of the $002_{NaCl}$ peak confirms that the increase of the formamide concentration in solution enhances as well the relative importance of the {111} surfaces and, ultimately, of the {111} growth sectors which are affected by the presence of absorbed layers of formamide. This, in turn, influences the value of the $<d_{001}>$ equidistance, according to relative portion of the {111} growth sectors which are intersected by the 001 lattice planes.

**iv$_{(002)}$** $C_f$ =100%, $T_{ev}$ = 30°C → As for the 111 peak, the shape of the 002 reflection, located at $<d_{001}>$ = 5.6238 Å becomes symmetric (Fig.12d,right side). Compared with the corresponding $<d_{001}>$ = 5.6106 Å value, calculated from the measured 111 peak obtained under the same growth condition (see **iv**$_{111}$), its deviation does not exceed –0.23%.

Summing up, from the detailed XRPD spectra carried out on the as grown NaCl crystals obtained in the presence of varying concentrations of formamide and having considered the related changes of their growth morphology, one can say:

*a*) – formamide easily adsorbs on the $\{111\}_{NaCl}$ surfaces, so generating the morphological transition: {100}→ {100} + {111}. This change was attributed to the adsorption of isolated formamide molecules on the {111} surfaces [10,33]. Through the observation of macrostep spreading on the {111} surfaces we found that formamide induces a K → F change in the character of the {111} form and, searching for lattice coincidences, we put forward the hypothesis of a 2D epitaxy setting up between the $101_{formamide}$ lattice planes and the $\{111\}_{NaCl}$ surfaces. Hence, the most reasonable model of formamide adsorption is not "random-molecular" but "2D-epitaxial islands".

*b*) – The thickness of the epitaxially adsorbed $d_{101}^{formamide}$ layers fits very well ($\Delta d << 5\%$) with the height of the elementary $d_{111}$ steps of NaCl crystals. Hence, one can reasonably suppose that the adsorbed layers can be easily buried in the $\{111\}_{NaCl}$ sectors during growth.

*c*) – XRPD spectra carried out on as grown NaCl crystal populations, under different temperature of crystallization and formamide concentration ($C_f$) in aqueous solutions, evidenced that the 111 and 002 reflections of NaCl are profoundly and differently modified

according to both temperature and ($C_f$) value, the main factor of change being the relative size of the "formamide contaminated" $\{111\}_{NaCl}$ growth sectors. This unambiguously proves our hypothesis put forward in (*b*).

*d*) – When NaCl crystals nucleate and grow from pure formamide solution, XRPD spectra indicate that only the {111} growth sectors exist in the crystals.

Then, we can conclude that "anomalous NaCl/formamide mixed crystals" forms in the {111} growth sectors only , at T >2°C and at different $C_f$ values in aqueous solutions. However, when $C_f$ =100%, then the "anomalous NaCl/formamide mixed crystals" occupies all the crystal volume, simulating the behaviour of a "homogeneous" crystal. This means that we have not to do, of course, with a solid solution but with NaCl crystals in which clusters of formamide layers are uniformly distributed in the growing crystals.

**References**


[1] A. Johnsen, *Neues Jahrb. Miner*. Bd.II (1903) 93

[2] P. Gaubert, *Bull. Soc. fr. Minéral*. 23 (1900) 211 ; 28 (1905) 180 ; 38 (1915) 149 ; 25 (1902) 242 ; *Comptes rendus* 167 (1918) 491 ; 180 (1925) 378 ; *Recherches récentes sur le faciès des cristaux*, Publ.Soc. Chimie Physique, Hermann, Paris (1911)

[3] A. Neuhaus, *Chemie der Erde*, 5 (1930) 529; 5 (1930) 554; *Z. Krist.*, 97 (1937) 28; 97 (1937) 112; 103 (1941) 297; 104 (1942) 197; 105 (1944) 161.

[4] H. Seifert, *Fortschr. Miner.* , 19 (1935) 103; 20(1936) 324; 22 (1937) 185.

[5] R. Kern, Bull. *Soc. fr. Minéral. Cristallogr.* 91 (1968) 247

[6] W. Kleber, Phys. Status Solidi (b) 2 (1962) 923

[7] E. Bauer, *Z. Kristallogr. Dtsch.*, 110 (1958) 372

[8] C.W. Bunn, *Proc. Roy. Soc.* , A141 (1933) 567

[9] L. Royer, *Comptes rendus* 198 (1934)185 ; ibid. 585 ; ibid. 949 ; ibid. 949 ; ibid. 1868

[10] M. Bienfait, R. Boistelle and R. Kern, in « Adsorption et Croissance Cristalline » Colloques Internationaux du CNRS n°152 (CNRS-Paris, 1965) 577

[11] a) - M. Bruno, D. Aquilano, L. Pastero, M. Prencipe, *Crystal Growth & Design* 8 (2008) 2163 ; b)- D. Aquilano, L. Pastero, M. Bruno, M. Rubbo, *J.Crystal Growth* 311 (2009) 399

[12] P. Hartman, in *Adsorption et Croissance Cristalline,* Colloques du CNRS n°152 (1965) 477

[13] R. Boistelle, G. Pèpe, B. Simon, A. Leclaire, *Acta Cryst.* B30 (1974) 2200

[14] S. Rajam, S. Mann, *J. Chem. Soc. Chem. Commun.* (1990) 1789

[15] I.V. Nefyodova, V.I. Lyutin, V.L. Borodin, P.P. Cvanski, N.I. Leonyuk, *J. Crystal Growth* 211 (2000) 458

[16] L. Pastero, E. Costa, M. Bruno, M. Rubbo, G. Sgualdino, D. Aquilano, *Crystal Growth Des. 4* (2004) 485

[17] L. Pastero, D. Aquilano, E. Costa, M. Rubbo, *J. Crystal Growth* 275 (2005) e1625.

[18] M .Bruno, M. Prencipe, *Surf. Sci.,* 601 *(*2007) 3012

[19] M. Bruno, D. Aquilano, M. Prencipe, *Crystal Growth & Design* 9 (2009) 1912

[20] L. Pastero, F.R. Massaro, D. Aquilano, *Cryst. Growth Des. 7 (*2007) 2749

[21] P. Hartman, R. Kern, *C.R. Acad. Sc. Paris* 258 (1964) 4591- 4593

[22] L. Pastero, D. Aquilano, *Cryst. Growth Des.* 8 (2008) 3451–3460

[23] F. Gille, K. Spangenberg, Z. Kris. Miner. Petrograd. A65 (1927) 204

[24] M. Bienfait, R. Kern, B. Mutaftschiev, Z. Krist. 120 (1964) 466

[25] N. Radenović, W.J. P. van Enckevort, J. Crystal Growth 234 (2002) 589

[26] N. Radenović, W.J. P. van Enckevort, P. Verwer, E. Vlieg, Surf. Sci. 523 (2003) 307

[27] N. Radenović, W.J. P. van Enckevort, E. Vlieg, J. Crystal Growth 263 (2004) 544

[28] N. Radenović, D. Kaminski, W.J. P. van Enckevort, S. Graswinckel, I. Shah, M. in 't Veld, R. Algra, E. Vlieg, J. Chem. Phys. 124, (2006) 164706

[29] N. Radenović, "The role of impurities on the morphology of NaCl crystals – An atomic scale view" PhD Thesis (2006) Radboud University Nijmegen

[ 30] J. Ladell , B. Post, Acta Cryst.7 (1954) 559

[ 31 ] T.Ottersen, Acta Chem.Scand. A 29 (1975) 939

[ 32] E.D. Stevens, Acta Cryst. B34 (1978) 544

[33] A. Singh, M.K. Kesharwani, B. Ganguly, *Crystal Growth & Design* 9 (2009) 77